

Supporting Information

Chen et al. 10.1073/pnas.1106420108

SI Materials and Methods

High-Level Expression of Human apoE3. A monomeric, biologically active, full-length human apoE3 is generated using an engineered pET30(+) vector (Novagen) in which the long his-tag in the N terminus was replaced by a short his-tag (eight histidines) as described (1). The expressions were carried out using *Escherichia coli* BL21(DE3) cells. The purification procedures essentially followed the manuals. Using high cell density method (2), we can routinely produce 17–30 mg isotope-labeled apoE3 in 100-mL minimum medium.

Preparation of Segmental Labeled apoE3 Proteins. The preparation of segmental labeled apoE using on-column native chemical ligation was following the protocol described previously (3).

NMR Spectroscopy Assignment. All NMR samples contained ~1 mM uniform/segmental triple-labeled human apoE3, in a buffer containing 100 mM sodium phosphate, at pH 6.8, 0.01 mM NaN₃, 10 mM EDTA, 10 mM *d*₁₀-DTT, 0.03 mM 4,4-dimethyl-4-silapentane-1-sulfonic acid (DSS), and 10% D₂O. For 3D/4D Nuclear Overhauser Effect Spectroscopy (NOESY) spectral collection, we used 50% deuterated triple-labeled apoE3 in 100 mM sodium phosphate, 500 mM urea at pH 6.8, 0.01 mM NaN₃, 10 mM EDTA, 10 mM *d*₁₀-DTT, 0.03 mM DSS, and 10% D₂O. All spectra were acquired at 30 °C on 600 MHz Varian INOVA spectrometer equipped with a cryogenic probe. Backbone assignment of full-length human apoE3 was achieved as described (4). HCC-TOCSY-NNH, CCC-TOCSY-NNH, 15N-edited NOESY and 4D ¹³C, ¹⁵N-edited NOESY were collected using a 50% deuterated triple-labeled apoE3 for the side chain atom assignment. NMR data were processed on a SGI workstation using nmrPipe (5) and the assignment was achieved using the PIPP and nmrvview software (6).

1. Zhang Y, et al. (2007) A monomeric, biologically active, full-length human apolipoprotein E. *Biochemistry* 46:10722–10732.
2. Sivashanmugam A, et al. (2009) Practical protocols for production of very high yields of recombinant proteins using *Escherichia coli*. *Protein Sci* 18:936–948.
3. Zhao W, Zhang Y, Cui C, Li Q, Wang J (2008) An efficient on-column expressed protein ligation strategy: application to segmental triple labeling of human apolipoprotein E3. *Protein Sci* 17:736–747.
4. Zhang Y, Chen J, Wang J (2008) A complete backbone spectral assignment of lipid-free human apolipoprotein E (apoE). *Biomol NMR Assign* 2:207–210.
5. Delaglio F, et al. (1995) NMRPipe: a multidimensional spectral processing system based on UNIX pipes. *J Biomol NMR* 6:277–293.

NMR Structure Determination. NOE distance restraints were generated using 3D/4D NOESY experiments, including 3D ¹⁵N-edited NOESY and 4D-¹³C, ¹⁵N-edited NOESY using both uniformly and segmentally labeled apoE3 samples. Unique segmental labeling strategy was developed using a ²H, ¹⁵N-apoE-NT-¹³C, ¹⁵N-apoE-CT sample. The 3D ¹⁵N-edited NOESY spectrum of this unique NMR sample allowed us to unambiguously identify 78 interdomain NOEs between apoE3-NT amide protons and apoE3-CT aliphatic protons (7). CSI program was used to predict secondary structure. TALOS program was used to obtain the backbone dihedral angles (ϕ and ψ based on chemical shift information (8).

A total of 3,459 NOE derived distance restraints, 408 dihedral angle restraints, and 318 hydrogen bond restraints were used for performing the structure calculation using the software package CYANA (9). Structure calculations were carried out in an iterative manner and each iteration generated and energy minimized 200 NMR structures in CYANA, including 10,000 steps of simulated annealing. The generated structures were analyzed for distance and dihedral angle restraint violations. A new restraint set was generated after these analyses for the next calculation. Final twenty best-fit NMR structures were used for further analysis.

Structural Analysis. The NMR structures of apoE3 were analyzed using Insight II (*MSI, San Diego*) and VADAR (10) programs. The VADAR provides the detailed information of buried hydrophilic residues, buried H-bonds, including the fractional solvent-accessible surface area of the side chain of each residue as well as H-bonds present in each structure. Insight II was used for superimposition and manual generating the apoE opening models based on structural and functional data of apoE. The structures are displayed using Pymol (*DeLano Scientific, Palo Alto*).

6. Johnson BA, Blevins RA (1994) NMRView: a computer program for the visualization and analysis of NMR data. *J Biomol NMR* 4:603–614.
7. Chen J, Wang J (2011) A segmental labeling strategy for unambiguous determination of domain-domain interactions of large multidomain proteins. *J Biomol NMR* 50:403–410.
8. Cornilescu G, Delaglio F, Bax A (1999) Protein backbone angle restraints from searching a database for chemical shift and sequence homology. *J Biomol NMR* 13:289–302.
9. Guntert P (2004) Automated NMR structure calculation with CYANA. *Methods Mol Biol* 278:353–378.
10. Willard L, et al. (2003) VADAR: a web server for quantitative evaluation of protein structure quality. *Nucleic Acids Res* 31:3316–3319.

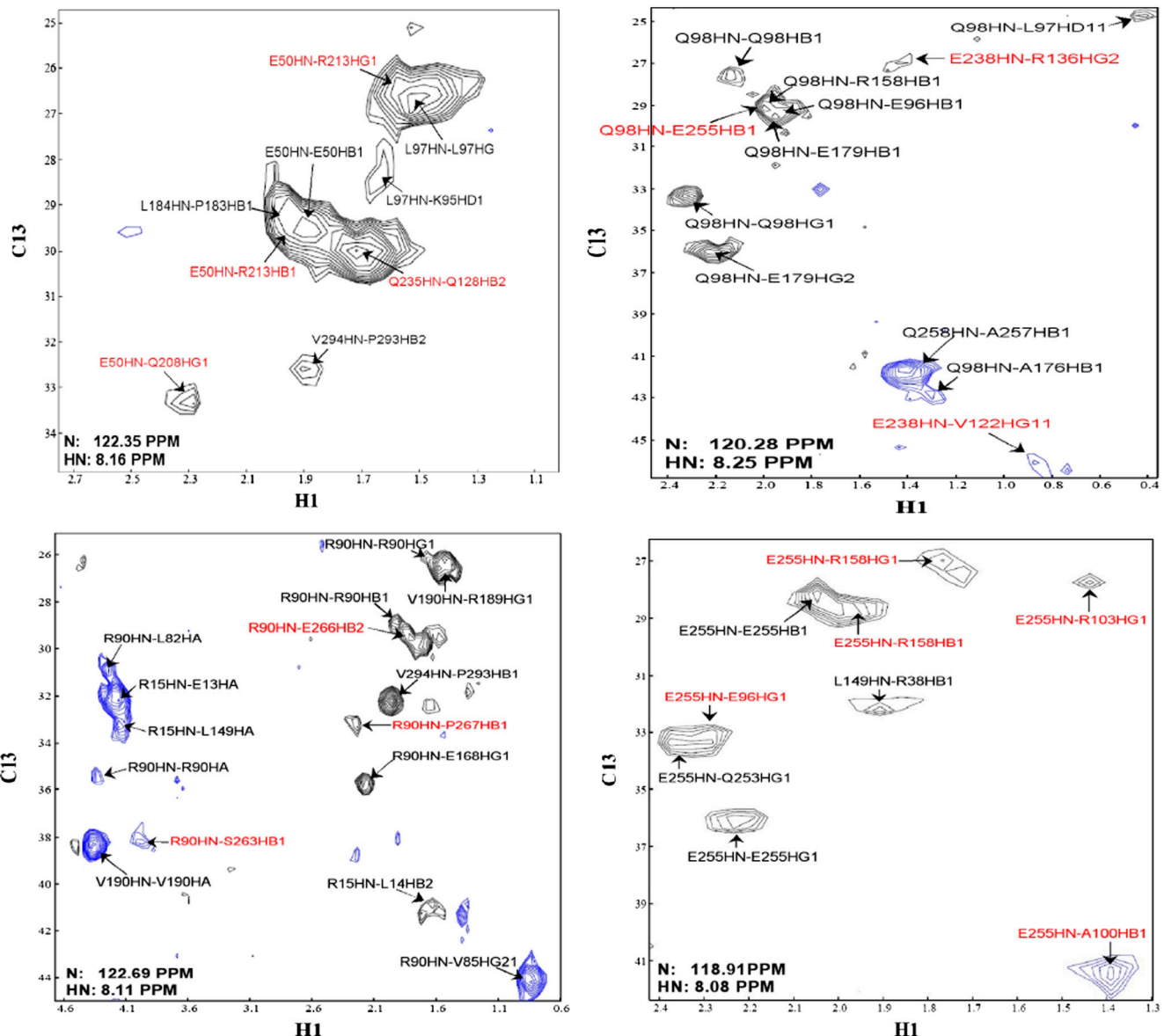


Fig. S1. Selected cross-sections of the 4D ^{15}N , ^{13}C -edited NOESY spectrum of apoE3. The ^{15}N and HN (amide proton) chemical shifts are labeled on each plane respectively. The spectral assignments are based on chemical shift assignment of apoE3 (BMRB database accession number: 15744). The crosspeaks labeled in red are long-range interdomain NOEs. The crosspeaks labeled in black are intradomain NOEs.

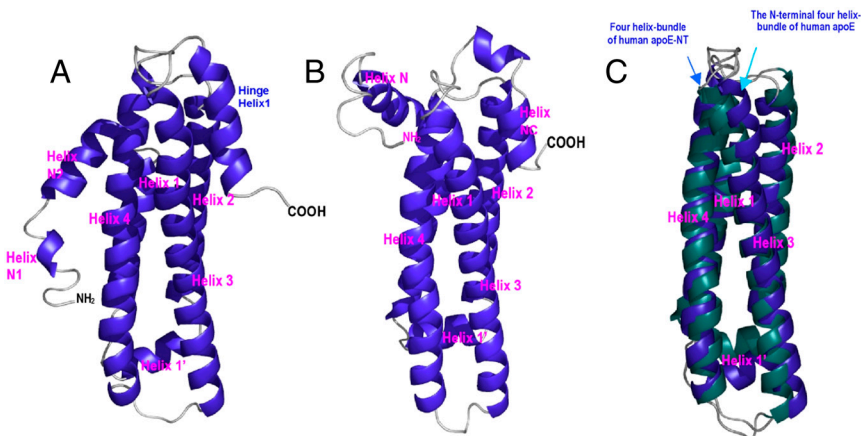


Fig. S2. A comparison of the NMR structures of the N-terminal domain of full-length apoE3 and apoE3(1–183). (A) NMR structure of the N-terminal domain of the full-length apoE3. (B) NMR structure of apoE3(1–183) (PDB accession code: 2kc3). (C) Superposition of the four helix bundle of the apoE-NT. The full-length apoE3 is colored in blue and apoE3(1–183) is green.

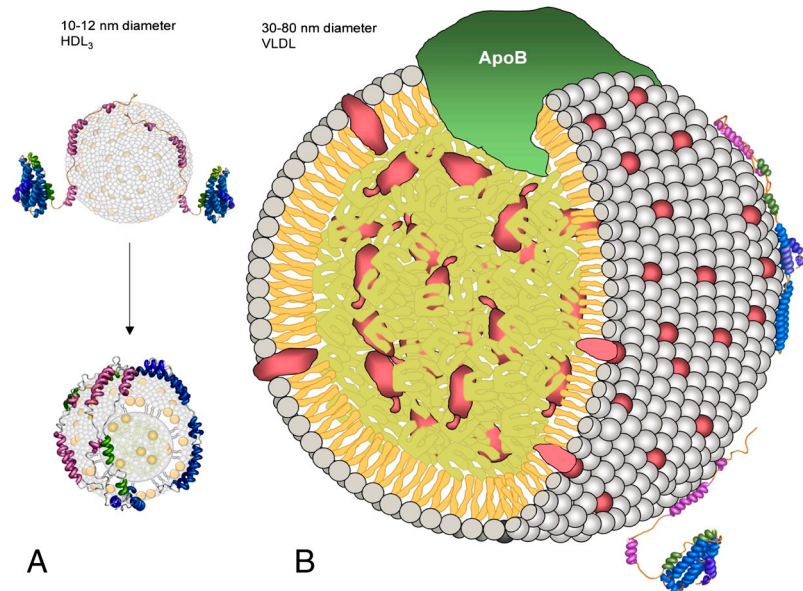


Fig. S3. Possible lipoprotein-associated apoE3 structures on HDL and VLDL particles. To simplify situation, we do not discuss apoAI and apoAII structures on spherical HDL particles. The diameters of the HDL (A) and VLDL (B) shown are 12 and 45 nm respectively. The apoE structures are shown in ribbons, with the apoE-CT in pink, the hinge domain in green, and the apoE-NT in blue, respectively. The surface-located cholesterol are shown with yellow balls in HDL and with purple balls in VLDL. The phospholipids are shown with gray balls in both HDL and VLDL. Triacylglycerols (TGs) are shown schematically in yellow whereas cholesterol-esters are shown schematically in purple inside the lipid-core of VLDL. Two states: a binding intermediate and a completely opened apoE conformation are shown to bind to both HDL and VLDL surfaces. In VLDL, we also showed apoB schematically.

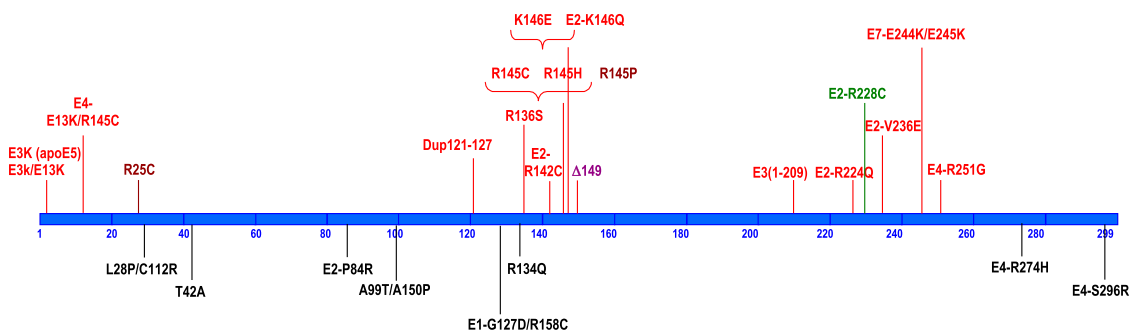


Fig. S4. Human Natural Occurring Mutants of apoE based on OMIM database.

Table S1. Structural statistics of the 20 best-fit NMR structures of human apoE3

Number of NMR restraints	
Total NOE restraints	3,459
Intraresidue	427
Sequential ($ i - j = 1$)	887
Medium range ($1 < i - j < 5$)	1,573
Long-range ($ i - j \geq 5$)	572
INTER-DOMAIN NOEs	224
Hydrogen bonds restraints	318
Total dihedral angle restraints	408
ϕ	204
ψ	204
Structural statistics	
Distance violations (>0.1 Å, %)	0.61
Average distance violations \pm rmsd	0.012 \pm 0.001
Dihedral angle violations (>2.5°, %)	0.31
Average dihedral angle violations \pm rmsd	0.311 \pm 0.059
Deviation from idealized geometry	
Bond lengths (Å)	0.00385 \pm 0.00018
Bond angles (°)	0.28308 \pm 0.01157
Improper (°)	0.06395 \pm 0.00242
Ramachandran plot (%)	
Residues in most favored regions	76.8
Residues in additional allowed regions	17.7
Residues in generally allowed regions	4.4
Residues in disallowed regions	1.1
Average pairwise rmsd (Å)	
All helix regions (13–22, 25–40, 45–52, 55–80, 89–125, 131–164, 168–180, 188–199, 209–223, 238–266, 271–276)	
Backbone heavy atoms	0.58 \pm 0.05
All heavy atoms	1.13 \pm 0.08
Long helix regions (25–40, 55–80, 89–125, 131–164, 238–266)	
Backbone heavy atoms	0.48 \pm 0.05
All heavy atoms	1.02 \pm 0.10
Superposition of the four helix-bundle between apoE and apoE N-terminal domain:	
(28–39, 56–79, 90–123, 132–162)	
Backbone heavy atoms	1.70

Table S2. Secondary structure locations of human apoE3

ApoE N-terminal domain:						
Helix N1 6–9	Helix N2 12–22	Helix1 26–40	Helix1' 45–52	Helix 2 55–79	Helix 3 89–125	Helix 4 131–164
ApoE Hinge domain:						
Hinge helix1 168–180	Hinge helix2 190–199					
ApoE C-terminal domain:						
Helix C1 210–223	Helix C2 236–266	Helix C3 271–276				

Table S3. Buried hydrophilic residues within apoE3 *

	LoopN (1–5)	HelixN1 (6–9)	HelixN2 (12–22)	Helix 1 (26–40)	Loop (41–44)	Helix 1' (45–52)	Helix 2 (55–79)	Loop (80–88)	Helix 3 (89–125)	Helix 4 (131–164)
ApoE-NT										
LoopN									R142, K146	
Helix N1										
Helix N2				E27					D153, Q156, K157	
Helix 1						T67, E70			Y118 [†]	
Helix 1'										
Helix 2				Y36					Y162	
Helix 3						Q55, T57, K75				
Helix 4	E3, Q4	T8	Q17, T18 S22						D107, R114 Y118	
The Hinge Domain										
HingeH1						E79			R90, S94, Q98 Q101	H140, D151
Hingeloop							Q55, T57, R61, D65, S197		C112, R119	
HingeH2										
ApoE-CT										
Helix C1				Q41, T42 S44	Q46, E49 E50, S53, S54, R213					R134,
Helix C2	R142, R146					R217	T83		T89, R92, E96, Q98, R103,D107 D110,E245 S263,E266 E238,K242 Q235	K143,R147 R150,D154 Q246 Q249,R264 D227,E234, Q235
Loop	T225									
Helix C3			Q275							D154,K157 R158, D271
LoopC	E281									S139 R150 Q279,E281 E287

*This table lists all the buried hydrophilic residues among apoE3 within the apoE-NT and between apoE domains. Based on orientations of these buried hydrophilic residues, we show them between the two helices. For example, S197 is between helices 2 and HingeH2

[†]The bold buried hydrophilic residues are between the two lobes of the allowed helix bundle opening of the apoE-NT (see Table S6, 11). The blue buried hydrophilic residues are between LoopN, Helices N1, N2, and Helix 4 that maintain the Loop N, Helices N1 and N2 in the defined position to interaction with Helix 4

Table S4. Hydrophobic residue distribution of the apoE-CT

Buried hydrophobic residues of the apoE-CT between apoE domains.
M221, T225, L229, A237, V239, L243, L252, A256, A259, V280, A291, V294.

ApoE-CT exposed hydrophobic residues
W210, L214, A216, M218, V232, V236, A241, A247, I250, A254, A257, L261, F265, L268, A269, M272, W276, A277, V283, A285, A286, T289, A292, P295, H299.

Table S5. H-bonds and salt-bridges within apoE N-terminal domain

LoopN (1–5)	HelixN1 (6–9)	HelixN2 (12–22)	Helix 1 (26–40)	Loop (41–44)	Helix 1' (45–52)	Helix 2 (55–79)	Loop (80–88)	Helix 3 (89–125)	Helix 4 (131–164)
Helix 1						W26-E70 L30b-T67 Y36-E59			
Helix 1'					E50-Q55				
Helix 2						R119-L52b			
Helix 3									
Loop (126–130)				T130-L43b					
Helix 4	R142-E3 K146-Q4	D153-L14b Q156-Q21 Q156-S22 K157-Q17		T130-S44b R145-Q41				L148b-D107 D151-A100b D151-L104b R158-E96 R172-S94 A176b-S94 E179-Q98	
HingeH1									

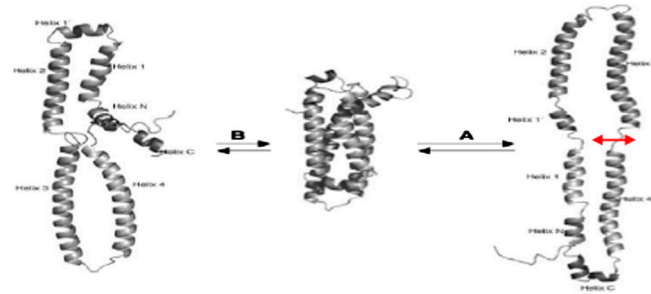


Table S6. A summary of published kinetic and thermodynamic data of lipid-free apoE3 and apoE3 interactions with lipid surface, lipoproteins and heparin and comparisons with our proposed two-step conformational adaptations of apoE3 upon binding to lipid surface, lipoproteins and heparin

Reference	Lipid emulsion [†]						Lipoproteins [§]						Heparin [¶]				ApoE3 conformational adaptations	
	Lipid-free *			DMPC *			Lipoproteins §			Heparin ¶								
	$\Delta G_{\text{H}_2\text{O}}$ (kcal/mol)	$\Delta G^{35/120}$ min ⁻¹	$\Delta H^{35/120}$ kcal/mol	$\Delta S^{35/120}$ kcal/mol	$K_d^{35/120}$ μM	K_m μM	k_1 min ⁻¹	k_2 min ⁻¹	K_d^{VLDL} μM	K_d^{HDL3} μM	k_{d1}	k_{d2}	K_1	K_2	K_α			
ApoE3	11–12	F/F	−12/ −11	−1.7/ −69	34/ −192	0.12/ 0.24	2.2	0.12	1.10	0.6 ± 0.1	4 ± 3	9.8	9.2	7.2	2.2	107	3.3	0.02
E3-CT	2–4	F/F	−11/ −12	−3.2/ −34	27/ −76	0.28/ 0.19	1.1	0.20	2.50	0.3 ± 0.1	0.5 ± 0.1	1.6	30	1.1	6.7	5.2	0.2	1.6
E3-NT	8–9	S/S	−10/ −10	−2.4/ −43	26/ −109	1.80/ 1.30	6.3	0.09	0.44	2.0 ± 1.8	1.7 ± 1.3	0.1	8.4	12	3.2	0.8	3.9	2.6
							4		5		6		7					

*The stability data of lipid-free apoE3 and two apoE3 domains are summarized from three publications listed in the column.

[†]Two different particles sizes of emulsion are reported in this publication, including 35 nm and 120 nm emulsion particles. The $k^{35/120}$ is the result of Fig. 1 of both particles in the cited publication. In the DMPC clearance time course of this publication, two phases of DMPC clearance were noted: Rapid phase and Slow phase. The k_1 and k_2 are the rate constants of rapid phase and slow phase respectively.

[§] K_d^{VLDL} and K_d^{HDL3} are the dissociation constants of apoE binding to VLDL and HDL3.

[¶] $k_{d1}(10^5 \text{ M}^{-1} \text{ s}^{-1})$, $k_{d2}(10^{-2} \text{ s}^{-1})$, k_{d1} and k_{d2} are the rate constants of association (a) and dissociation (d) of first step and second step binding of apoE to heparin using a two-step mechanism proposed in the cited publication. $K_1(10^5 \text{ M}^{-1})$ and K_2 are the binding constants of apoE to heparin of first step and second step. $K_\alpha (\mu\text{M})$ is the overall dissociation constant.

^{||}The apoE3 conformational adaptation is also two steps which is described in the text. This two-step conformational adaptation of apoE3 upon lipoprotein-binding and heparin-binding is based on specific structural topology of apoE3, providing a unique and specific mechanism of apoE3 interacting with lipoproteins including HDL and VLDL and with heparin/HPSG. This two-step conformational adaptation of apoE3 provides details of the structural rationale of apoE3 in response to lipoprotein-binding and heparin-binding.

- Wetterau JR, Aggerbeck LP, Rall SC, Jr., Weisgraber KH (1988) Human apolipoprotein E3 in aqueous solution. I. Evidence for two structural domains. *J Biol Chem* 263:6240–6248.
- Clement-Collin V, et al. (2006) The structure of human apolipoprotein E2, E3 and E4 in solution. 2. Multidomain organization correlates with the stability of apoE structure. *Bioophys Chem* 119:170–185.

3 Morrow JA, et al. (2006) Differences in stability among the human apolipoprotein E isoforms determined by the amino-terminal domain. *Biochemistry* 39:11657–11666.

4 Saito H, et al. (2001) Lipid binding-induced conformational change in human apolipoprotein E. Evidence for two lipid-bound states on spherical particles. *J Biol Chem* 276:40949–40954.

5 Segal ML, et al. (2002) Influence of apoE domain structure and polymorphism on the kinetics of phospholipid vesicle solubilization. *J Lipid Res* 43:1688–1700.

6 Nguyen D, Dhanaisekaran P, Phillips MC, Lund-Katz S (2009) Molecular mechanism of apolipoprotein E binding to lipoprotein particles. *Biochemistry* 48:3025–3032.

7 Futamura M, et al. (2005) Two-step mechanism of binding of apolipoprotein E to heparin: implications for the kinetics of apolipoprotein E-heparan sulfate proteoglycan complex formation on cell surfaces. *J Biol Chem* 280:5414–5422.